The Morro Vermelho hypogenic karst system (Brazil)

Stratigraphy, fractures, and flow in a carbonate strike-slip fault zone with implications for carbonate reservoirs

Bertotti, Giovanni; Audra, Philippe; Auler, Augusto; Bezerra, Francisco Hilario; de Hoop, Stephan; Pontes, Cayo; Prabhakaran, Rahul; Lima, Rebeca

DOI
10.1306/05212019150

Publication date
2020

Document Version
Final published version

Published in
AAPG Bulletin

Citation (APA)
Bertotti, G., Audra, P., Auler, A., Bezerra, F. H., de Hoop, S., Pontes, C., Prabhakaran, R., & Lima, R. (2020). The Morro Vermelho hypogenic karst system (Brazil): Stratigraphy, fractures, and flow in a carbonate strike-slip fault zone with implications for carbonate reservoirs. *AAPG Bulletin*, *104*(10), 2029-2050. https://doi.org/10.1306/05212019150

GEOLOGIC NOTE

The Morro Vermelho hypogenic karst system (Brazil): Stratigraphy, fractures, and flow in a carbonate strike-slip fault zone with implications for carbonate reservoirs

Giovanni Bertotti, Philippe Audra, Augusto Auler, Francisco Hilario Bezerra, Stephan de Hoop, Cayo Pontes, Rahul Prabhakaran, and Rebeca Lima

ABSTRACT

The Morro Vermelho Cave (MVC) (Brazil) developed within the Morro Vermelho karst system, which affected Neoproterozoic limestones (Salitre Formation). The MVC experienced little interactions with meteoric processes and is an example of a hypogenic cave formed during strike-slip deformation. The Salitre carbonates in the MVC experienced distributed deformation along an elongated domain overlying a buried strike-slip fault. Gently dipping, semiductile shear zones formed with decimeter-scale (3.9 in.) dolomitic veins. In our model, Mg-rich fluids flowing along the Salitre aquifer caused at the same time extensive dolomitization of the body of rock (100-m [328-ft] scale) experiencing distributed deformation. With progressive displacement, the deep strike-slip fault propagated upward causing the development of an anticline pop-up, steepening sedimentary layers, and steep 1–10-m-long (3.3–33.8-ft) fractures, which served as pathways for upward fluid flow. These steep extensional fractures made it possible for fluids flowing in lower, quartzitic aquifers to enter the carbonate aquifer causing silica deposition in rock cavities and in fractures and fault planes. Following the main stage of speleogenesis, silica deposition took over again depositing

Manuscript received June 13, 2019; provisional acceptance August 8, 2019; revised manuscript received September 4, 2019; revised manuscript provisional acceptance November 4, 2019; 2nd revised manuscript received December 14, 2019; final acceptance May 21, 2020.
DOI:10.1306/05212019150

AUTHORS

GIOVANNI BERTOTTI ~ *Department of Geoscience and Engineering, Delft University of Technology (TU Delft), Delft, the Netherlands; g.bertotti@tudelft.nl*

Giovanni Bertotti is a geology professor at TU Delft. He holds an M.Sc. in geology and a Ph.D. from ETH Zurich. From 1991 to 2011 he worked at Vrije Universiteit Amsterdam focusing on the deformation of sedimentary basins. Since 2012, Giovanni has worked at TU Delft where he has developed a research line on multiscale analysis of fractured reservoirs. He is the corresponding author of this paper.

PHILIPPE AUDRA ~ *Polytech Lab Unité Propre de Recherches 7498, University of Nice Sophia Antipolis, Nice, France; audra@unice.fr*

Philippe Audra is a professor in the Engineering School of the University of Nice Sophia Antipolis, France. His studies focus on speleogenesis (cave origin and evolution, especially hypogene caves), late-stage processes such as condensation–corrosion, and karst aquifer dynamics and resources. His published contributions are on many karst areas of the planet such as China, Papua New Guinea, Philippines, and Europe.

AUGUSTO AULER ~ *Instituto do Carste, Carste Ciência e Meio Ambiente, Belo Horizonte, Minas Gerais, Brazil; aauler@gmail.com*

Augusto Auler is a consultant and runs a private company specializing in environmental geology. His research interest are mostly related to karst landscapes, including hydrogeology, speleogenesis, paleoclimate, and geomorphology. He performs research through collaborative arrangements with universities and colleagues from many parts of the world.

FRANCISCO HILARIO BEZERRA ~ *Federal University of Rio Grande do Norte, Natal, Rio Grande do Norte, Brazil; bezerrafh@geologia.ufrn.br*

Francisco H. Bezerra is a professor at the Department of Geology, Federal University of Rio Grande do Norte, Brazil. His studies focus on fractures and faults, stress fields, and

analogs of oil reservoirs. His published contributions include the tectonic evolution of sedimentary basins along the east and equatorial margins of Brazil and Precambrian basins in the Brazilian cratonic area.

Stephan de Hoop ~ *Department of Geoscience and Engineering, Delft University of Technology, Delft, the Netherlands; s.dehoop-1@tudelft.nl*

Stephan de Hoop is a Ph.D. candidate at TU Delft. He has a background in civil engineering (bachelor's degree) and petroleum engineering (master's degree). His main research interests are in numerical methods for fluid flow simulation, uncertainty quantification, and understanding the complex chemical fluid–rock interactions in karst systems.

Cayo Pontes ~ *Federal University of Rio Grande do Norte, Natal, Rio Grande do Norte, Brazil; cayopontes@gmail.com*

Cayo Pontes received his M.S. degree in oil and mining exploration at the Universidade Federal de Campina Grande and is currently working on his Ph.D. at the Universidade Federal do Rio Grande do Norte. His research areas include structural geology, mechanical stratigraphy, and petrophysics properties applied in analogue reservoirs.

Rahul Prabhakaran ~ *Department of Geoscience and Engineering, Delft University of Technology, Delft, the Netherlands; r.prabhakaran@tudelft.nl*

Rahul Prabhakaran is a Ph.D. student at TU Delft. He is working on fracture network characterization, focusing on image processing methods for fracture data acquisition and quantitative metrics for network description.

Rebeca Lima ~ *Federal University of Rio Grande do Norte, Natal, Rio Grande do Norte, Brazil; rebeca.seabra@hotmail.com*

Rebeca Lima is a Ph.D. candidate at University of Rio Grande do Norte, Brazil. She has a background in geology (bachelor's degree) and geophysics (master's degree). Her main research interests are stratigraphy and diagenesis in Neoproterozoic carbonate caves, understating the stratigraphic and structural control between carbonate layers and porosity

on the cave walls a continuous silica crust, rarely observed in other settings worldwide. The interplay between regional bedding-parallel flow and focused circulation of fluids along steep faults and dipping layers, and the associated rock–fluid interactions are not unique to the contractional settings presented but can also occur in association with similar faults in rifted continental margins.

INTRODUCTION

Hypogenic karst is related to permeable structures enlarged by dissolution associated with upwelling fluid flow independent of recharge from the overlying or immediately adjacent surface (Klimchouk, 2007, 2012). The aggressive character of these upwelling fluids is usually acquired from deep-seated sources of CO_2 and, not alternatively, H_2S, possibly associated with thermal processes, and is independent of soil or meteoric acids (Palmer, 2000; Audra and Palmer, 2015). Karst systems have long been known as an important factor in carbonate reservoirs for hydrocarbons as well as for geothermal energy (Goldscheider et al., 2010; Burchette, 2012). In the last years, there has been an increasing interest in these systems because of the discovery that dissolution is commonly related to the rise of chemically aggressive hypogene fluids rather than to meteoric waters (Feng et al., 2017; Zhu et al., 2017; Reijmer et al., 2018), one of the most important implications being that some karsts might have formed at depth rather than at the surface. The underground voids (caves) provide the (connected) pores for the high to superhigh permeability streaks characterizing, among others, the subsalt play of offshore Brazil (Carlotto et al., 2017) and geothermal reservoirs in Paleozoic carbonates in northwest Europe (Reijmer et al., 2018). At the same time, karst poses significant engineering and flow management challenges because it can cause the loss of drill bits and unexpected water breakthrough and earlier-than-expected arrival of cold-water front in the case of geothermal doublets. Because these voids are commonly too small to be visible in seismic data (see, however, Basso et al., 2018 for a notable exception) and too big to be characterized on the basis of wells, there is a great need for tools to predict their position, shape, size, and distribution in the subsurface and to implement them in reservoir simulators.

Because hypogenic fluids essentially move across the stratigraphy, their flow is controlled not only by the primary and diagenetic permeability of the sedimentary layers but also by the presence and spatial organization of fracture corridors, faults, and distributed fractures (Klimchouk, 2017). Large faults and fracture corridors, especially when subvertical, favor efficient upward movement of aggressive fluids without significant heat loss. Extensive networks of distributed fractures, however, favor lateral

flow and widespread dissolution, especially when fractured layers are sealed by less permeable units (Cazarin et al., 2019). The development of hypogenic caves is indeed controlled by the complex interplay between fluid chemistry and physics and by the sedimentologic and structural architecture of the affected rocks (Klimchouk, 2017).

Outcrops (including caves and associated karst systems accessible from the surface) form an outstanding source of information to strengthen our ability to predict the architecture and development of hypogenic caves, as well as their relationship with observables such as stratigraphy and tectonic structures. In caves, lithologic properties can be described and measured, structures such as faults and fracture corridors likewise can be constrained, and cements of veins can be investigated. The three-dimensional (3-D) nature of cave passages allows for the observation of features at different angles, and the general lack of weathering favors the preservation of features that would otherwise be obliterated in surface outcrops (Plotnick et al., 2015). All these parameters can then be used for better understanding of long-term, regional-scale flow patterns.

In this contribution, we report on our findings from the Morro Vermelho (MV) karst system (MVKS) associated with the MV Cave (MVC), a remarkable and previously undocumented cave located in the Irecê Basin (Bahia State, Brazil) (Figure 1). The MVC is also quite unique because, differing from the numerous caves in the Irecê Basin, the composing carbonate layers are fully dolomitized and steeply dipping. Differing from most hypogenic caves, more recent speleogenesis did not mask or completely obliterate evidence of older phases in the MVC, whereby clear mineralogical and structural evidence is still available, providing clues about the little-known earlier stages of deformation, void generation, and mineral deposition.

The cave developed in Neoproterozoic carbonate units of the Salitre Formation (Fm.) affected by a steep fault zone. The MVKS is clearly linked to fractures and faults, thereby presenting a relevant case study for hypogenic caves where aggressive fluids moved upward and laterally along fracture corridors, faults, and tilted sedimentary layers. Using modern techniques of portable LIDAR, we document for the first time the geometry and development of substantial hypogene dissolution along a fault zone and along steepened sedimentary layers. We show how interactions between conduit generation (fracturing, dissolution) and infilling (precipitation of minerals in fractures and voids) are key for the understanding of multiscale permeability in carbonate reservoirs.

Following a geologic introduction, we present the detailed geometry of the cave derived from innovative LIDAR tools, and we describe and interpret the speleological architecture, the structural geology of the cave, and the associated veins, eventually integrating these observations in an evolutionary model for tectonic and fluid-flow evolution.

formation, especially the main porosity that originates the cave passages.

ACKNOWLEDGMENTS

This research was carried out in association with the ongoing R&D project registered as ANP 20502-1: "Processos e Propriedades em Reservatórios Carbonáticos Fraturados e Carstificados – POROCARSTE3D (UFRN/UnB/UFRJ/UFC/Shell Brasil/ANP) – PoroKarst – Processes and Properties in Fractured and Karstified Carbonate Reservoirs", sponsored by Shell Brasil under the ANP R&D levy as "Compromisso de Investimentos com Pesquisa e Desenvolvimento." We thank the Brazilian Federal Environmental Agency, Instituto Chico Mendes, for providing the license to study and sample the caves. Candidates Rahul Prabhakaran and Stephan de Hoop acknowledge support from the Molengraaff Funds and the Topsectoren Kennis & Innovatie geo-energy project CarbFrac. We thank P. de Wolff (Geometius) for allowing us to rent geo simultaneous localization and mapping for LIDAR acquisition and sharing with us his knowledge, A. Jordão (Carste Ciência e Meio Ambiente) for efficiently taking care of our safety during cave activity, David Lopes Castro for the geophysical images, and Murilo Valle for providing initial information on this very interesting cave.

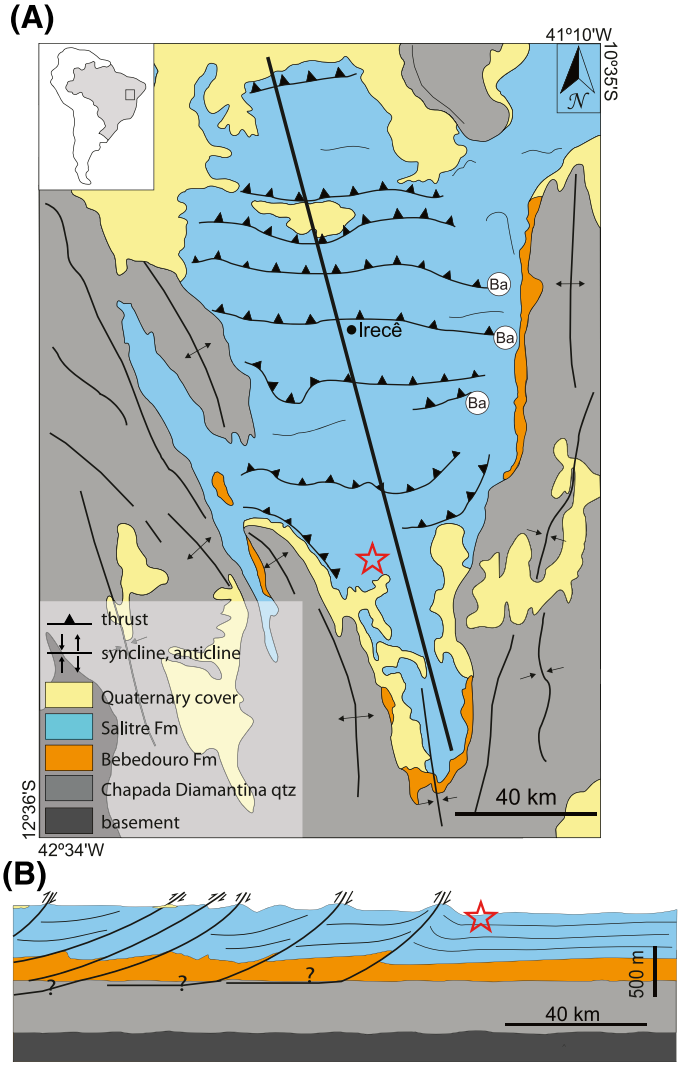

Figure 1. The regional setting of the Morro Vermelho karst system. (A) Map of the Irecê basin (simplified from Reis et al., 2013); (B) geological section across the basin (trace indicated with thick line in map). Black arrows indicate displacements. The red star as shown in panels (A) and (B) indicates the position of the Morro Vermelho Hill. The black lines are undefined structural lineaments. Ba = barite mineralization; Fm = Formation; qtz = quartz.

THE OVERALL SETTING

Regional Geology and Geography

The MVKS developed within the Neoproterozoic limestone of the Salitre Fm., within the Irecê Basin (Figure 1) (Misi and Veizer, 1998). The Salitre carbonate overlies the Mesoproterozoic pelite of the Bebedouro Fm., the Mesoproterozoic quartzite of the Chapada Diamantina Group (Magalhães et al., 2016), and an Archean crystalline basement (Trompette et al., 1992).

The carbonates of the Salitre Fm. are presently preserved in an inverted rift basin bounded to the west and east by two anticlines exposing quartzites of the Chapada Diamantina Group (Figure 1A). To the south, the same quartzite outcrops in the young relief of the Chapada Diamantina (e.g., Japsen et al., 2010), which forms the southern boundary of the carbonates. The carbonates of the Salitre Fm. are affected by east-west–trending thrusts and fault-related folds associated with north-south shortening of the Brasiliano orogeny (740–650 Ma) (de Almeida et al., 2000; Sampaio et al., 2001) (Figure 1). The intensity of contractional deformation decreases southward and carbonates in the study area are generally flat lying (Figure 1B).

Toward the west and east, these thrusts merge in approximately north-south–trending lateral ramps, which

have a dextral and sinistral sense of movement, respectively. Sulfur mineralization (e.g., barite) that has not been analyzed yet is associated with these transcurrent faults, suggesting intense fluid circulation of chemically loaded fluids (Sampaio et al., 2001) probably after passing through the Bebedouro tillite. Alternatively, sulfur could originate from sulfide beds (mostly Fe and Zn sulfides) that occur at depth in the Salitre Fm. (Misi and Kyle, 1994) and disseminated pyrite, which has been commonly observed in specific layers of the carbonates.

The carbonates of the Salitre Fm. presently support a low-altitude and low-relief area surrounded to the east, west, and south by the mountains of the Chapada Diamantina, with quartzites layers generally dipping toward the low-elevation domain. Currently, meteoric waters flow along the flank of these hills and enter the carbonate succession, causing widespread meteoric karstification and epigenic caves draining eventually toward the Santo Antônio River, which acts as the current base level of the area (Laureano et al., 2016).

The Morro Vermelho Cave and Karst System

The MVKS is associated with the approximately 50-m-high (~164-ft) east-west–trending MV Hill (1.2 × 0.4 km [0.7 × 0.2 mi]), which forms an unusual relief emerging from the otherwise flat landscape composed of soil- and laterite-covered flat-lying carbonates of the Salitre Fm. (Figure 2A). The hill is generally covered by silicified blocks (Figure 2B) that preserved the relief but obscure the bedrock, which is only observable inside the cave, in small scattered outcrops in the MV Hill and in a nearby hill.

The entrance to the cave is marked by a narrow vertical passage located on the northern side of the hill (Figure 2). From there, a small passage descends toward the southwest for 15–20 m (49–65 ft) before joining the main chamber, which is characterized by a fairly irregular geometry (Figure 3). From this chamber, the cave passage splits into different levels, one continuing down toward the southeast as steep passages and fracture-guided shafts and one rising toward the northwest. The bottom of the cave approximately corresponds to the altitude of the plain. To the south of the main chamber, the cave continues with a north-northeast–south-southwest passage for another few meters. The floor of the passages is composed of rubble, fine-grained sediments derived both from the weathering of the bedrock and outside sources, and organic material from bat colonies and animals that use the cave as a den.

The cave displays no features such as fluvial sediments, dendritic or anastomotic pattern, or fluvial speleogens, which would be associated with fluvial action. The walls of the cave are mostly covered by a thick and an unusual silica crust, partly detached as a consequence of meteoric

Figure 2. The Morro Vermelho Hill. (A) Aerial view of the Morro Vermelho looking toward the south; the hill is approximately 50 m (~164 ft) high and 1.2 km (0.74 mi) long (photograph courtesy of R. Maia). (B) Silicified pebbles and blocks covering the entire hill; the image is 2 m (6.5 ft) across.

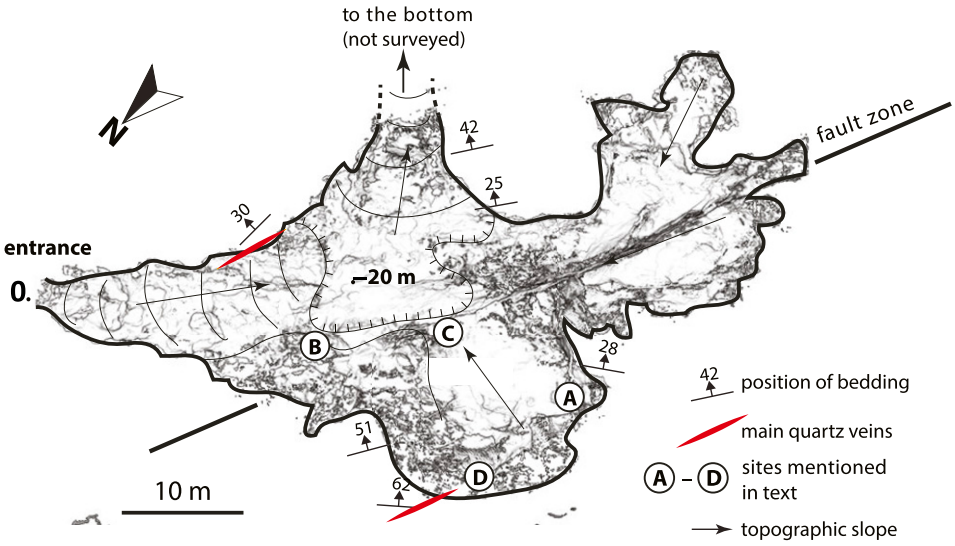

Figure 3. Plan view of the surveyed passages of the Morro Vermelho Cave. The backdrop of the picture is formed by the LIDAR model. The map is enriched by speleological and structural (position of bedding, veins) information. The hatched line is a morphologic step in the cave. The depth of the reference point is –20 m (65 ft) with respect to the cave entrance (0.); thin solid lines are qualitative isodepths.

action (Figure 4). Despite the partial masking of the cave bedrock by chemical coatings, a variety of structural features and mineralizations (fractures, veins, and faults) can be observed and will be described in the following sections.

THE GEOMETRY OF THE MORRO VERMELHO CAVE

The LIDAR Survey

Constraining the full 3-D geometry of caves has been a major challenge until a few years ago, preventing a detailed and quantitative estimate of, for instance, dissolved volumes and of shape changes along cave tunnels. Adopting a recently developed technology, we have produced one of the first full 3-D digital models of complex caves using geo simultaneous localization and mapping (GeoSLAM) ZEB REVO®, a handheld mobile mapping system able to rapidly generate 3-D point clouds of the cave interior (Zlot and Bosse, 2014). The GeoSLAM ZEB REVO is a light, easily portable unit composed of a laser range scanner coupled with an inertial measurement unit (IMU) mounted on a rotating drive generating in real time point clouds while the operator walks through the cave. The device uses a 3-D simultaneous location and mapping algorithm to fuse the two-dimensional laser scan data with the IMU data to generate the 3-D point clouds (Bosse et al., 2012; Zlot and Bosse, 2014). For the purposes of this study, GeoSLAM is superior to conventional terrestrial laser scanning because it does not require the bulky equipment and cumbersome setups that are ill suited for cave environments, where narrow and tortuous passages make stop-and-scan strategies difficult. Such systems are, however, possibly adapted for smaller caves or specific parts of larger caves (De Waele et al., 2018).

We covered the largest part of the MVC, approximately 80 m (~262 ft) long and 30 m (98 ft) wide, in five different surveys with varying degrees of overlap, with a total survey time of approximately 1.5 hr. Smaller parts could not be surveyed because passages were too narrow or the descent was too steep. The volume of the analyzed MVC is approximately 3000 m^3 (~10,600 ft^3).

The point cloud of each survey was subsequently registered and aligned to the cave map, which included the position of the cave entrance. Point cloud registration can be done in several ways, but we found the workflow defined in the manual of the open-source software CloudCompare, version 2.9 (CloudCompare, 2019), to be the most effective: (1) use manual translations and rotations to approximately align each individual survey to the

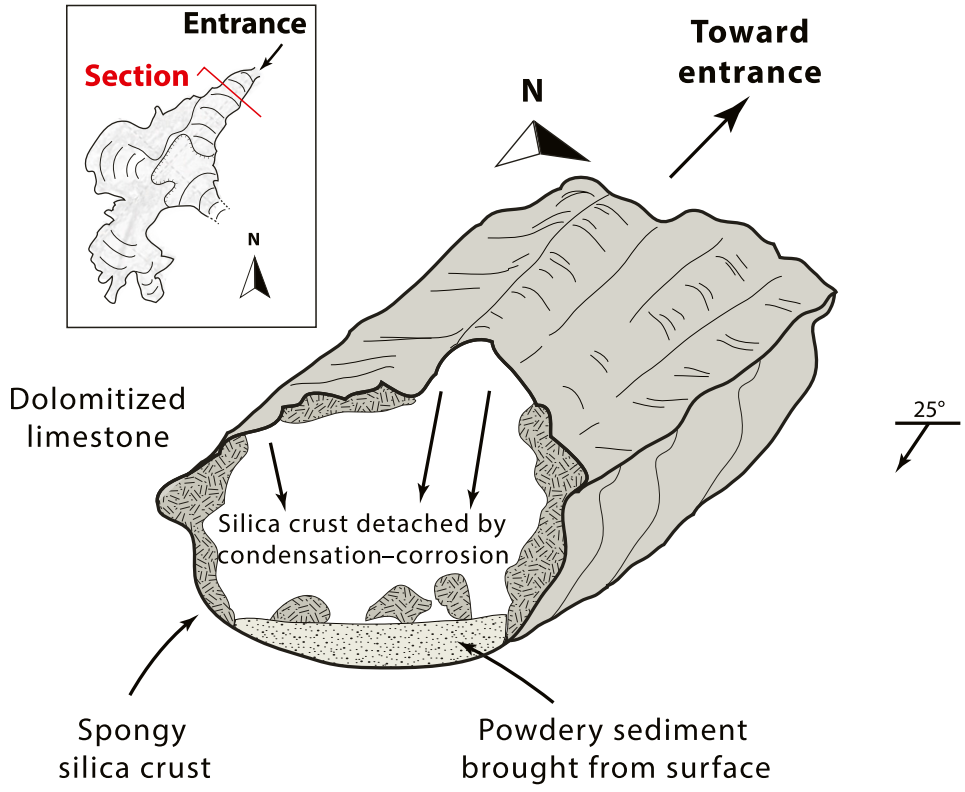

Figure 4. Schematic view of the main speleological features of the Morro Vermelho Cave.

reference survey, (2) extract a small subset of each individual survey which has clearly overlapping points, (3) apply iterative closest point (ICP) (Besl and McKay, 1992) to finely register these subsets to the reference cloud, (4) apply the obtained transformation matrix from the ICP to the full point clouds to obtain the fully aligned surveys, and (5) merge the aligned individual surveys together and obtain one full continuous survey of the cave.

After all surveys were aligned and merged, a continuous survey of the cave was obtained comprising approximately 20.7 million points. The resolution, or point density, of the acquired LIDAR data varies spatially and is mainly controlled by the distance between the measurement device and the object of interest and by the exposure time. The detection limit of features, when using the ZEB REVO, approximately follows a 1:10 ratio, (e.g., a feature of size 10 cm [3.9 in.] can still be recognized at a distance of 1 m [3.3 ft] between the measurement device and the feature of interest). Where needed, resolution was improved by increasing exposure time, looping several times over the same section, possibly lowering the operating speed, thereby mapping previously unmapped surfaces.

The results of the survey produced a detailed 3-D model in a very time-efficient manner. Because of the high resolution obtained, the 3-D model can be used to map and determine the position in space of geological features such as bedding and faults, commonly with a precision higher than that achieved with a traditional compass. In addition, the full 3-D cave model can be easily used for further analysis and experiments such as geomechanical simulations.

Geometry: Results

The map view extracted from the LIDAR survey provides an accurate and informative description of the main part of the MVC (Figure 5).

The model clearly shows the irregular shape of the cave with the northeast-southwest–trending main elongation axis and the passages toward the southeast and northwest. The model also clearly images a sharp linear feature striking North 20 (N-20) (bottom left to top right in Figure 5), which corresponds to the

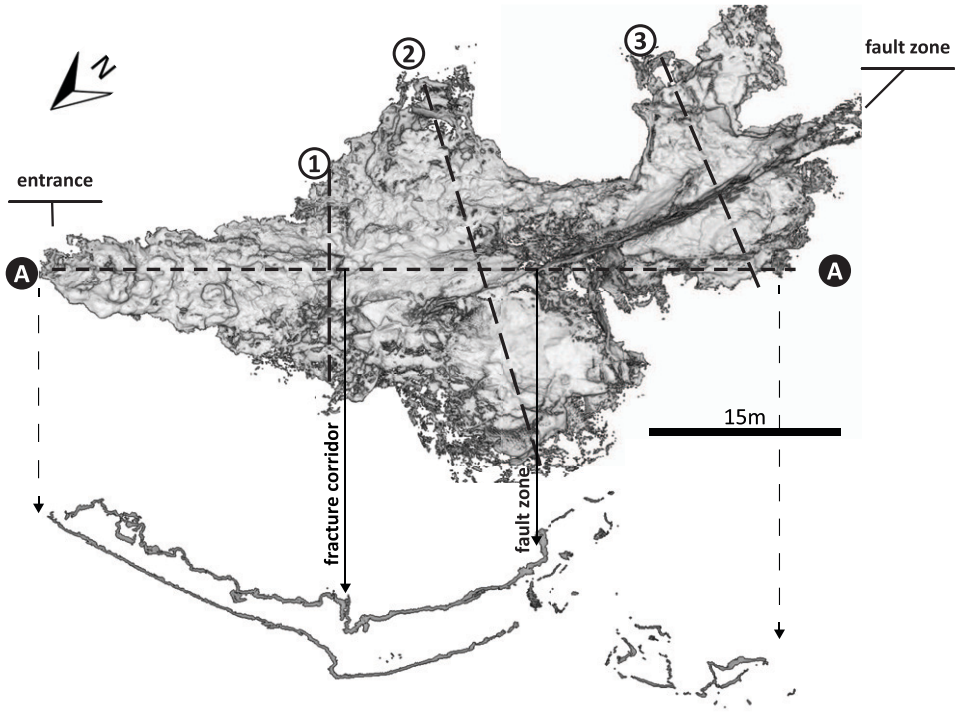

Figure 5. The LIDAR model of the Morro Vermelho Cave. Upper panel: plan view of the digital model showing the ceiling data points projected on a flat horizontal surface; traces 1 to 3 refer to the transversal sections shown in Figure 6. Lower panel: vertical section along the main axis of the cave (trace A).

subvertical karstified fault zone with veins, which forms a major component of the architecture of the MVC.

A transect across the point cloud in a direction parallel to the cave axis (Figure 5B) shows the northern entrance passage descending toward the southwest, eventually reaching the main chamber where the cave floor is relatively flat. The morphology of the cave is marked by two sharp vertical steps associated with a fracture corridor (on the left) and with the main fault zone of the cave (Figure 5). The step visible on the right-hand side of the section is an artifact related to the intersection between the transect and the cave walls.

Sections in northwest-southeast direction, at high angle to the cave axis and to the strike of sedimentary beds, display the eastward-deepening shape of the cave, conditioned by the position of the sedimentary

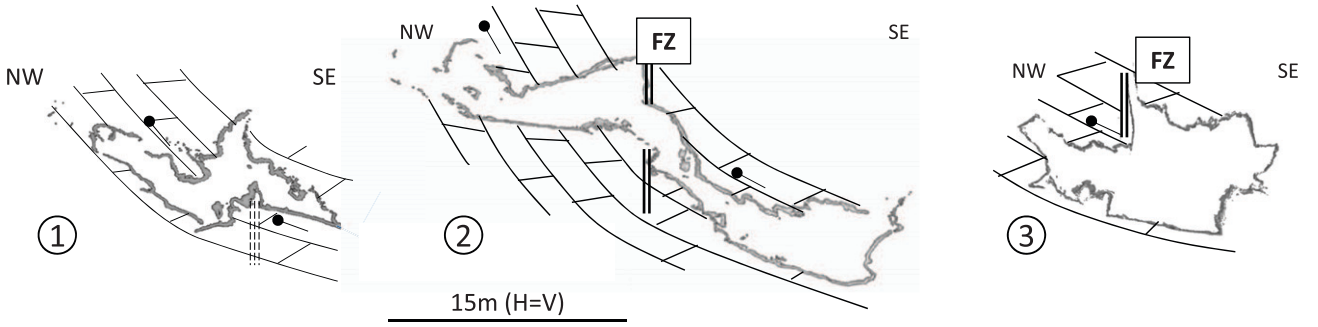

Figure 6. Transects across the LIDAR model of the Morro Vermelho Cave at high angle to the cave elongation (see Figure 5 for their location). Short lines with bullet termination indicate the position of bedding as measured in the cave walls. Note the clear morphological expression of the fault zone (FZ) in the roof of the cave along transects 2 and 3 and the fracture corridor in transect 1. H = horizontal; V = vertical.

layers (Figure 6), and highlight the factor of stratigraphy in controlling speleogenesis. In transect 1, the cave is composed of two segments parallel to sedimentary bedding separated by a steep zone coinciding with a fracture corridor. Cave morphology in transect 2 is more complicated, with a subhorizontal segment in the northwest passing to the southeast to a passage generally dipping parallel to bedding (Figure 6B). The transition between the two is formed by the main fault zone. In the third transect, the cave has a fairly irregular shape with the cave floor dipping parallel to bedding. The trace of the fault zone is clearly visible in the roof of the cave (Figure 6C).

STRUCTURAL GEOLOGY AND MINERALIZATION IN THE MORRO VERMELHO KARST SYSTEM

Country Rock

As the cave dips on the whole parallel to the bedding, only 10–15 m (33–49 ft) of stratigraphy are exposed. Detailed observations are also made difficult by the widespread presence of a siliceous crust in the cave walls. In general, lithologies exposed in the cave are composed of fine-grained limestone organized in centimeter- to few decimeter-thick layers (tenths of inch to several inches). The country rock visible in the MVC and everywhere in the hill is fully dolomitized.

A unique feature of MVKS is represented by the inclined position of the sedimentary layers, very different to most of the other caves of the region, where layers are essentially horizontal. Dips are approximately 30° to the east-southeast in most of the cave but become as high as 60° in the westernmost domains where dips are to the southeast (Figure 7). We interpret the changes in bedding dip as related to a fold with a north-northeast–trending fold axis.

Distributed En Echelon Veins

Systems of en echelon centimeter-scale veins (0.5 to 1 in.) are observed in the walls of the main chamber and at the southern part of the northeast-southwest passage (Figure 8A). Vein infill is dolomitic. The walls of the veins are sharp and regular, documenting the lack of dissolution prior to cement precipitation.

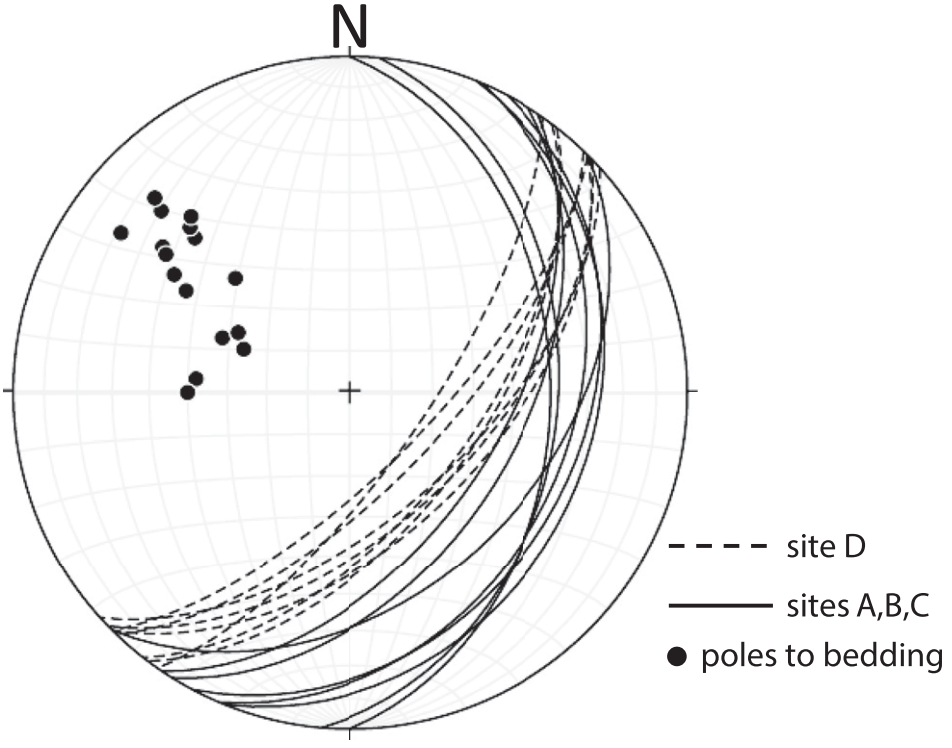

Figure 7. Lower hemisphere projection of bedding in the Morro Vermelho Cave. Letters refer to sites in Figure 3.

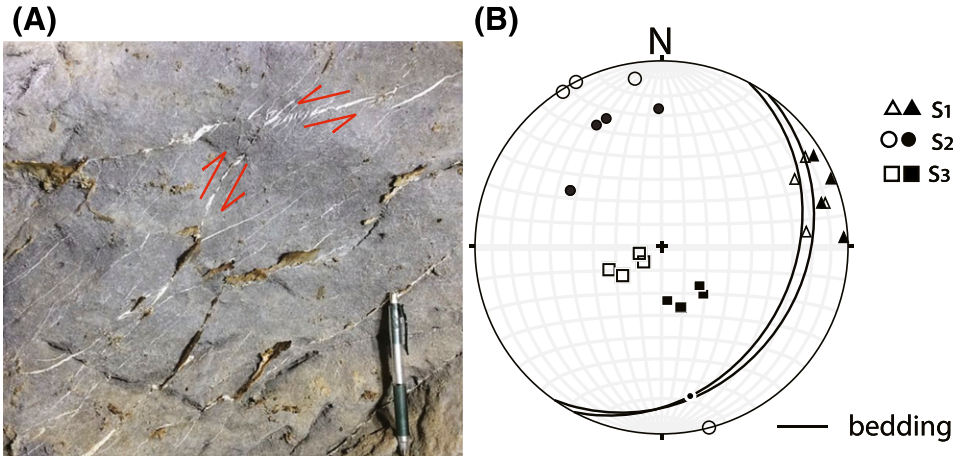

Figure 8. En echelon veins. (A) Photograph from the cave wall. Red arrows indicate sense of movement along shear zones. (B) Stereoplot (lower hemisphere projection) with principal stresses (maximum principal stress [S_1] > intermediate principal stress [S_2] > minimum principal stress [S_3]) derived from four sets of conjugate semiductile shear zone (greater than two shear zones per set and ~20 veins); hollow and solid symbols refer to the present-day and back-rotated position of principal stresses.

The veins form semiductile shear zones organized in conjugate sets (Figure 8A) at low angle with respect to bedding. The conjugate nature of these shear zones is confirmed by interfault angles of 50°–60° and by the sense of movement inferred by the en echelon veins. Therefore, these sets provide reliable estimates of the direction of the principal stresses during deformation. Notwithstanding the difficulties of measuring these subtle features in the flat cave walls and using the standard Anderson approach, we derived directions of principal stresses from three sets of semiductile shear zones. The results are consistent and indicate maximum principal stress (σ_1) dipping approximately 20° to the east-northeast and an intermediate principal stress (σ_2) subhorizontal and trending north-northwest–south-southeast (Figure 8B). The σ_1 lies on the bedding plane, suggesting that the deformation took place prior to layer steepening.

Steep Veins and Barren Fractures

Rocks visible in the MVC are also affected by widespread steep barren fractures and planar veins with quartz infill. Because of their steep position and infill mineralogy, these veins are clearly different from the en echelon veins described above. Steep veins strike generally north-northeast–south-southwest (Figure 9A) and are typically centimeters to decimeters long (tenths to several inches) and centimeters thick (~0.1 to 1 in.). In thin sections, quartz in the veins sometimes has a blocky texture, but fibers are also common and develop at a high angle to the fracture wall (Figure 9B). Barren fractures have a consistent north-northeast–south-southwest strike fully overlapping that of quartz veins (Figure 9A).

The position of quartz veins and steep barren fractures is constant throughout the entire cave (Figure 3), independent of the position of bedding. Because of the overlapping position and common extensional character, we interpret quartz veins and barren fractures to have formed during the same deformation stage, after the steepening of sedimentary layers. As a consequence of differential dissolution, veins form blades and a structure of boxwork protruding from the cave walls documenting their formation prior to speleogenesis.

Faults

Some surfaces observed in the MVC present striations and are thus interpreted as faults. Their directions range from north-south to northeast-southwest, with generally steep dips toward the west-northwest and east-southeast (Figure 10). All faults have a normal fault character, sometimes with a strike-slip component. Paleostress analysis performed using the Win-Tensor program (Delvaux and Sperner, 2003) suggests that all faults can be explained by a normal fault regime with a subvertical σ_1, a σ_2 (corresponding to the

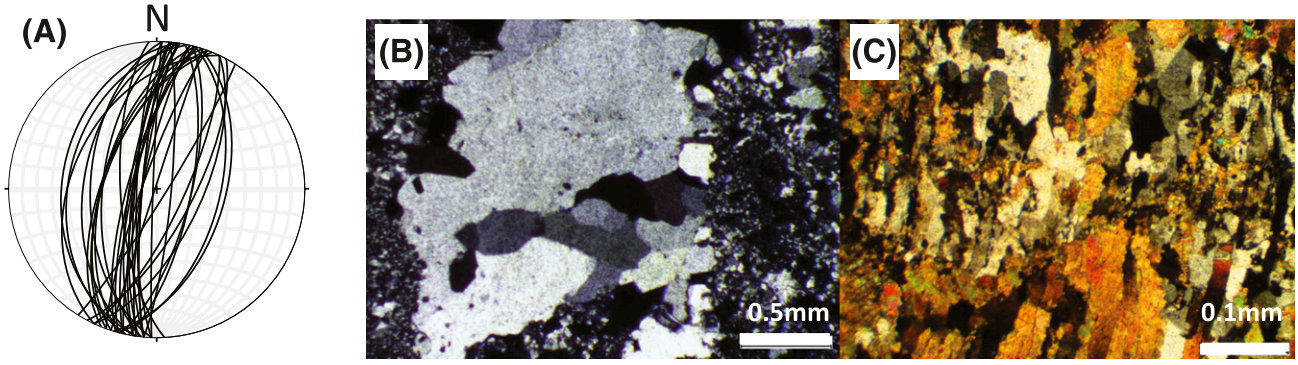

Figure 9. Steep veins and barren fractures. (A) Stereoplot; veins and fractures formed after layer tilting and therefore have not been back rotated. (B) Thin sections (crossed nicols) of veins; note quartz infill with a fibrous texture (sample number CARB0090). (C) Fibrous quartz (sample number CARB0094) (crossed nicols).

maximum horizontal stress) directed northeast-southwest, and a northwest-southeast–trending minimum principal stress (σ_3) (Figure 10). Fault positions are not correlated to that of bedding; therefore, we assume that they developed during the late stages or following the steepening of sedimentary layers.

Based on their similar directions, we suggest that faults are in fact reactivations of the steep veins and barren fractures, both accommodating extensional strain. The correlation between faults and steep veins is also strengthened by the fact that crystals growing along faults are, similarly to the vein infill, composed of quartz.

Fault Zone

A dominant feature of the MVKS is a tens-of-meters-long N-20 planar structure clearly visible in map view and in the vertical transects of the LIDAR model (Figure 5). The structure is a complex feature composed of slip surfaces and a thin fault gouge, barren fractures with evidence of dissolution, and decimeters-thick quartz veins. These features are parallel to each other and parallel to the steep quartz veins, with associated barren fracture discussed in previous sections and independent on the position of layers, suggesting that they all formed approximately at the same time after tilting.

Silica Crusts

The cave walls are characterized by the presence of an unusual silica crust (Figure 11). This crust can be up to 50 cm (20 in.) thick and can display a spongy texture with high porosity (Figure 11A–C) or be quite massive. This silica crust is now falling apart because of processes of corrosion by water condensation on the dolomite that supports them. Silica also occurs as masses of silica spherulites growing on silica spongy crust. Silica is also locally present as small pockets in the bed rock partially replacing dolomite crystals and documenting the limited interactions between SiO_2-rich fluids and the dolomitic country rock (Figure 11).

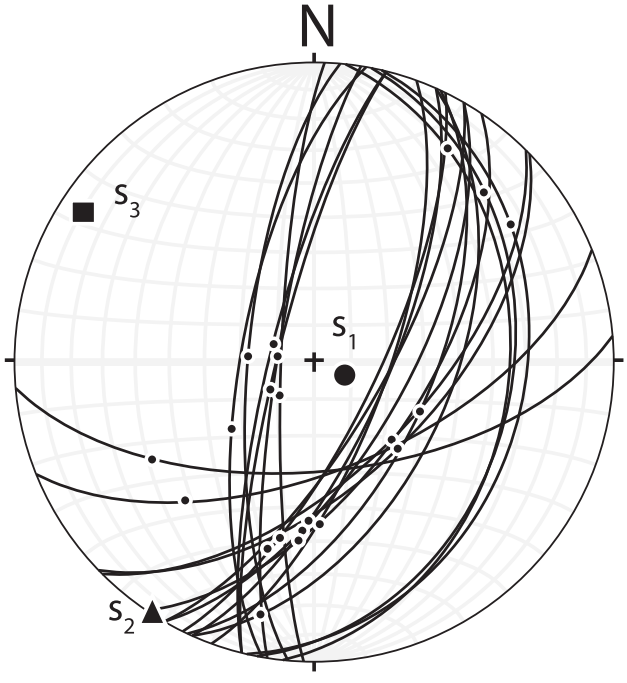

Figure 10. Faults, striations, and paleostress analysis from fault in the Morro Vermelho Cave; analysis performed with the Win-Tensor program. S_1 = maximum principal stress; S_2 = intermediate principal stress; S_3 = minimum principal stress.

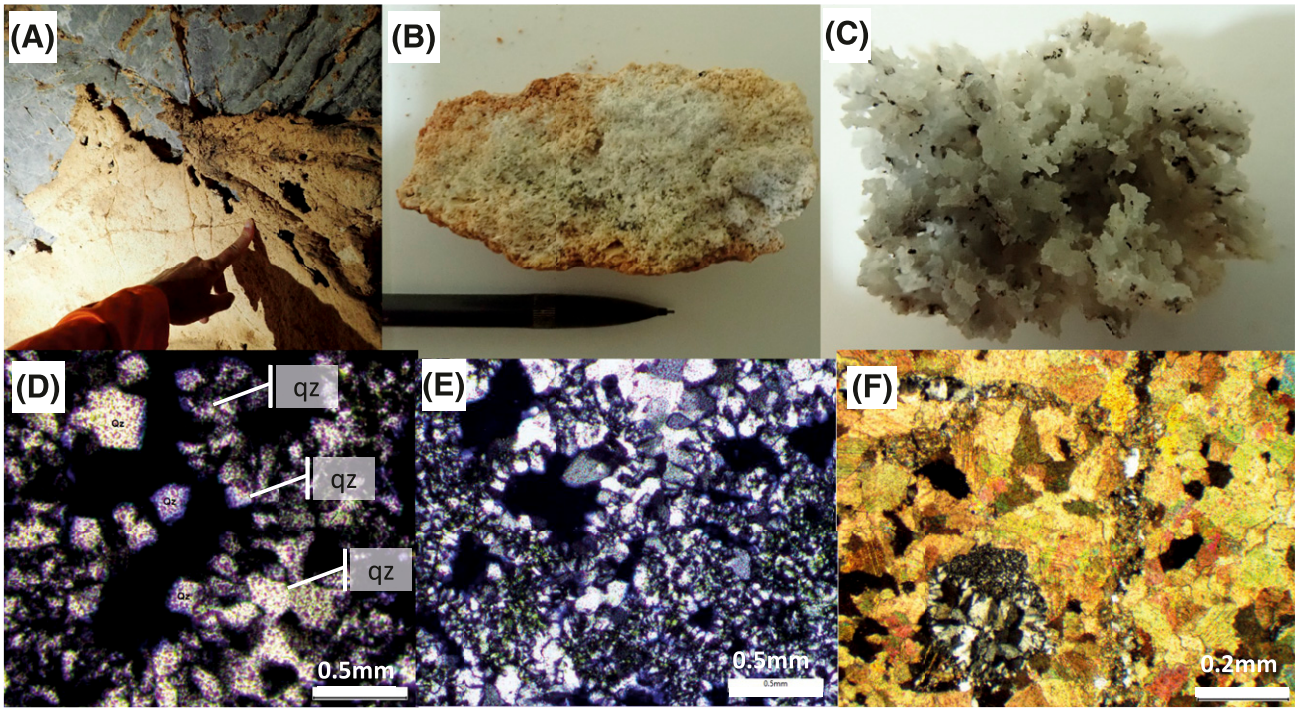

Figure 11. Silica deposition on Morro Vermelho Cave walls. (A) Image of the cave wall, the lower light part corresponding to the silica crust. The upper gray part corresponds to the dolomite host rock, visible after detachment of silica crust. Note the fractures highlighted by recent condensation–corrosion. (B, C) Closer views of the silica sponge crust. Central sample is 9 cm (3.5 in.) long. Right view (C) is approximately 3 mm (~0.1 in.) wide; note the branchlike growth of mineralization. (D) Thin section (crossed nicols) showing quartz (qz) replacing rhombohedric dolomite crystals (sample CARB0090). (E, F) Thin sections (crossed nicols) of quartz precipitated in cavities in the dolomite close to the cave walls.

FLUIDS AND SPELEOGENESIS

Observations

A key element for the understanding of the genesis of the MVKS is constraining the origin of the fluids that caused the dissolution of the Salitre carbonates and, thereby, the formation of the MVC. Like it is commonly the case in speleological studies, this hinges on the identification of diagnostic morphological features preserved in the cave walls (Audra et al., 2009).

The absence of features such as sinking streams or vadose shafts associated to recharge from the surface and the lack of fluvial sediments and associated fluvial speleogens (such as scallops) suggest that meteoric runoff was a negligible factor in the initial formation of the MVC. On the contrary, several diagnostic morphostructures have been observed that are supportive of a hypogenic origin of the MVC, that is, of dissolution associated with the rising of chemically aggressive fluids rather than meteoric fluids.

The cave presents a very irregular 3-D pattern made of large chambers separated by narrow passages, which generally develop by volume expansion in a context of slow rising flow (Osborne, 2001). Narrow vertical passages occur at the bottom of the cave (not visible on the incomplete survey in Figure 3), which are parallel to the main fault of the MVC and which are generally interpreted as feeders providing pathways for rising fluids (e.g., Klimchouk, 2007). Ceiling cupolas are circular dissolution features associated with slow convective flow of condensation–corrosion and are nicely developed in the upper reaches of the MVC (Figure 12A, D). Finally, the walls and the ceiling of the cave are marked by protruding bodies corresponding to the infill of quartz veins and resulting from the differential corrosion between the more soluble dolomite country rock and the very hard silica veins. Millimetric veins may protrude for several centimeters (up to a few inches), whereas the

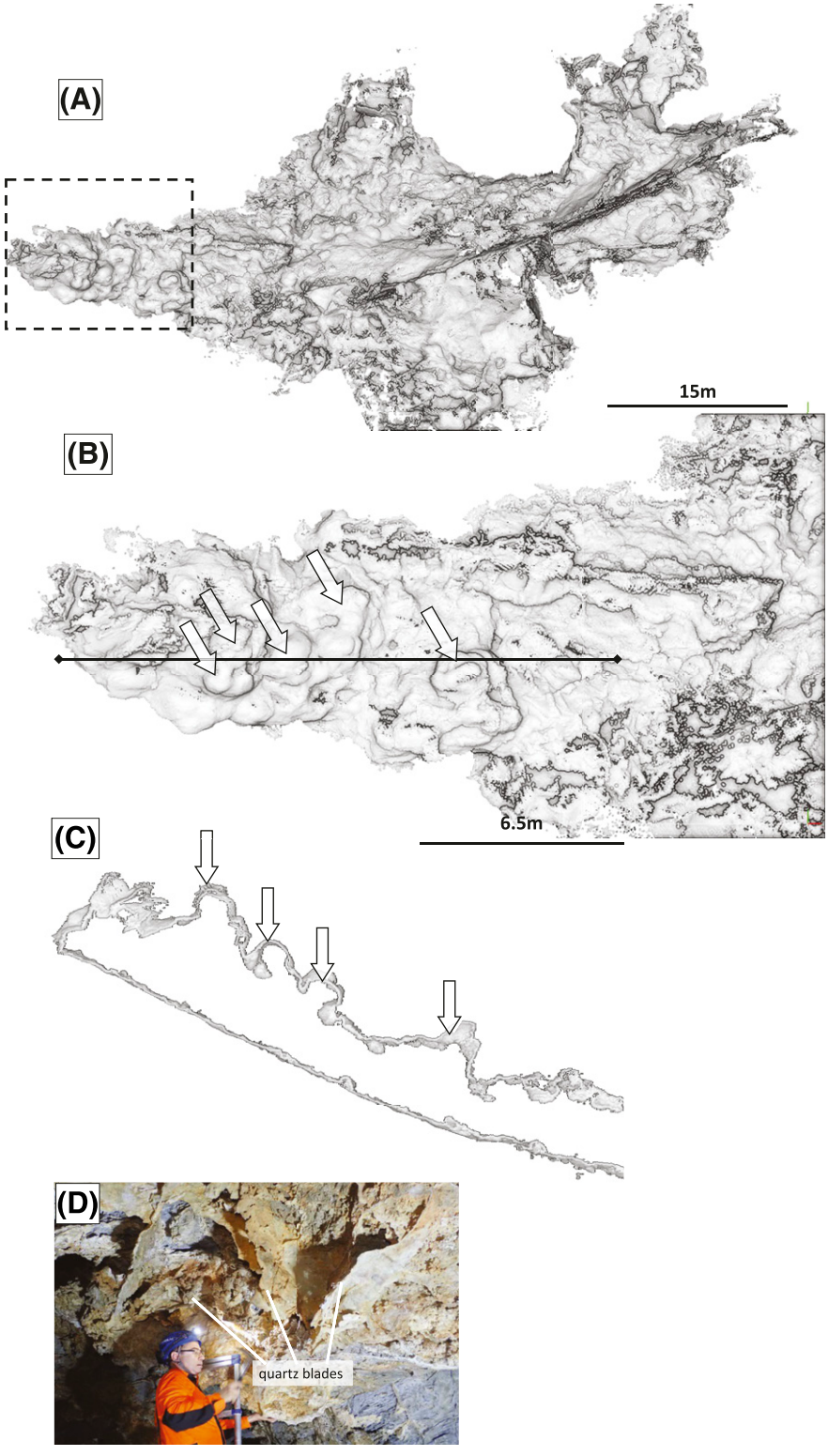

Figure 12. Morphostructures diagnostic of hypogenic (upward) flow. (A–C) The cupolas extracted from the LIDAR survey in map view (A, B) and in vertical section (C). White arrows point to the cupolas. (D) View of the boxwork developed in the ceiling of the main chamber: The 1-mm (0.04-in.)-thick silica veins (light planar surfaces) are protruding for half a meter (1.6 ft) and encompass the dolomite country rock (in gray), which is also silicified at the scale of the microporosity. White arrows point to arrow blades. Francisco Hilario Bezerra is pictured for scale.

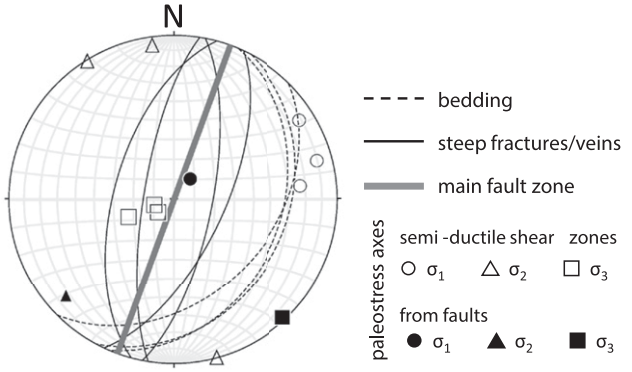

Figure 13. Summary of all relevant structural elements observed in Morro Vermelho Cave. σ_1 = maximum principal stress; σ_2 = intermediate principal stress; σ_3 = minimum principal stress.

thickest veins protrude for half a meter (1.6 ft) (Figure 12C). These protrusions range among the largest observed ever in caves. Even if this boxwork (as these patterns are named in speleological jargon) can be present in other settings mainly because of meteoric condensation–corrosion, it is very frequent and extended in the hypogenic environment.

The most diagnostic feature, however, is extensive silica crust that covers large parts of the walls, except in places where they detached after condensation–corrosion of the underlying dolomite country rock (Figures 4, 11A). Silica crust thickness is highly variable but can reach in places up to half a meter (~1.6 ft). The transition with the underlying dolomite country rock is gradual, with impregnation of silica replacing the dolomite crystals (Figure 11D–F). Such extensive silica replacement crust is a very uncommon feature in carbonate environment.

A deep origin of the fluids associated with the development of the MVC is compatible with the fact that the mineralogical assemblage (mainly silica) observed in the cave is unrelated to meteoric sources of acidity related to atmospheric and soil-derived H_2CO_3, which would instead result in low-temperature $CaCO_3$-related precipitates (i.e., mainly calcite speleothems), as it is the case in most of the caves in the Irecê Basin.

A Speleogenic Model

In our interpretation, the cave was formed by fluids flowing from deep sources focused upward along the fracture corridors and fault zones such as the ones we have documented, which acted as conduits within a phreatic environment. Rising fluids were also channelized along the steepened sedimentary beds following layers of higher permeability, related to sedimentary and diagenetic processes possibly coupled with higher fracture densities. Our preliminary data suggest that fractures were a more important factor than primary rock porosity.

DEFORMATION AND FLUID FLOW IN THE MORRO VERMELHO KARST SYSTEM

Evolution of the Morro Vermelho Karst System

The MVKS is characterized by the abundance of deformation structures typically associated with precipitation and, possibly, dissolution phenomena. This allows for a fairly detailed reconstruction of its structural evolution and of cave speleogenesis, fluid flow, and fluid–rock interactions through time (Table 1). Although the relative chronology of the different stages is broadly established, the lack of suitable datable material prevents the precise bracketing of events in terms of absolute ages.

Stage 1: Distributed Deformation and Dolomitization

A first stage of fluid circulation led to the diffuse dolomitization of a body of rock that was hundreds of meters (several hundreds of feet) thick, in any case, larger than the volume of the MVKS. Our interpretation that wholesale dolomitization was associated with fluids rising along the steep strike-slip faults and not, for instance, to seawater during early diagenesis (e.g., Hollis et al., 2017), is essentially based on the fact that fully dolomitized carbonates are only found in the MV Hill and do not exist in the entire region.

During or following wholesale dolomitization, the rocks of the MVKS experienced distributed deformation leading to the development of extensive systems of en echelon veins organized in conjugate sets of semiductile shear zones. The geometry of these shear zones documents a stress field characterized by a bedding-parallel, east-northeast–west-southwest–trending σ_1 and a bedding-perpendicular (subvertical) σ_3 (Figure 13). The en echelon veins are spread over the entire cave and represent, therefore, a stage of distributed deformation probably affecting

Table 1. Proposed Evolutionary Scheme for the Morro Vermelho Karst System

Stage		Structures	Rock–Fluid Interactions	Character
1:	Distributed deformation	Semiductile shear zones (en echelon veins)	Bedrock dolomitization and dolomite precipitation in en echelon veins associated with Mg-rich fluids	Hypogenic
2:	Layer tilting	–	–	Hypogenic
3:	Formation of steep extensional fractures	Long and steep, extensional fractures	Deposition of SiO_2 in veins and along fault planes associated with rising Si-rich fluids	Hypogenic
4:	Speleogenesis	–	Dissolution by rising chemically aggressive (H_2CO_3?) waters	Hypogenic
5:	Deposition of silica crust	Some possible reactivation of steep fractures	Deposition of silica crust by partial replacement of the dolomite walls associated with Si-rich fluids	Hypogenic
6:	Draining of the cave and connection to surface processes	Some possible reactivation of steep fractures	Disintegration and alteration of dolomite, detachment of silica crusts caused by condensation–corrosion	Epigenic

Abbreviation: – = not applicable.

a large body of rock up to 10 m^2 (33 ft^2) laterally hosting the MVKS.

The Mg-rich fluids, possibly the same that caused wholesale country rock dolomitization, precipitated dolomite in the en echelon veins. No large subvertical veins with dolomite infill have been detected in the MVC, and tension gashes are typically less than a couple of decimeters (several inches) in dimension and are not interconnected; these observations suggest that flow occurred mainly along the carbonate layers of the Salitre Fm. rather than across it, essentially using the primary and diagenetic permeability of the carbonates, locally enhanced by semiductile shearing.

Indirect evidence on the depth of the MV rocks during this stage of deformation can be derived from the knowledge that, in the presence of a tectonic stress, the σ_3 can only be vertical at relatively shallow depths. Based on modeling work by Bertotti et al. (2017) predicting depths at which the σ_2 is vertical, we estimate that the MVKS during the development of tension gashes was not more than 500–800 m (1600–2600 ft) below the Earth's surface.

Stage 2: Tilting

Following the development of semiductile distributed deformation, the sedimentary layers were steepened probably in association with an approximately north-northeast–trending anticline. We have no information as to the width of the fold. The inferred fold axis is oblique (angle of 40°–60°) to the direction of maximum compression associated with the semiductile shear zones (Figure 13), suggesting that if semiductile shearing and steepening occurred under the same boundary conditions, folding developed in a strike-slip rather than in a pure shear setting.

Stage 3: Steep Extensional Fractures and Silica-Filled Veins

Rocks of the MVKS were then affected by the formation of barren fractures and veins that were steep, decimeters to several meters (feet to tens of feet) long, and predominantly extensional. Veins and barren fractures have a fairly consistent north-northeast–south-southwest–trending orientation with dips both to the northwest and southeast. Parallelism between steep fractures and bedding direction suggests that the steep fractures opened in association with folding. Slickensides on the quartz infill of the veins document normal and strike-slip faulting, all related to an extensional stress regime with subvertical σ_1 and subhorizontal, east-northeast–west-southwest–trending σ_2 (Figure 13). The fault zone apparent in the cave and in the LIDAR model is one of these features that accommodated more displacement and opening than the others.

The quartz infill of the steep veins documents the circulation of fluids fundamentally distinct from those documented during stage 1. Flow of SiO_2-rich fluids was confined to the fracture system, causing no significant bedrock silicification and imposing a predominant upward flow component. Because the silica is widespread in surface outcrops in MV Hill (away from the cave), but not in a nearby hill, we interpret precipitation as being caused by a focused episode of rising SiO_2-rich fluids, which promoted widespread silicification in veins and faults along the rising path.

A high temperature of the fluids is suggested by the fact that precipitation rates of silica from fluids cooler than 100°C is very low (Lowell et al., 1993). Mixing with cooler (meteoric?) water bodies and contact with the cooler bedrock could provide optimal conditions for silica deposition (Rimstidt and Barnes, 1980; Martin and Lowell, 2000). Because we cannot assume thermal equilibrium between the fluids and the country rock, we cannot use fluid temperature to estimate the depth of the MVKS during the development of SiO_2 extensional veins. Their occurrence during anticline development suggests that rocks were shallower than during stage 1.

Stage 4: Speleogenesis

During stage 4, the cave formed characterized by irregular chambers, vertical rifts, and other morphological features indicative of ascending speleogenesis (Klimchouk, 2009). We have no direct evidence of the chemical composition of the causative acidic fluids. We believe that fluids involved mostly an H_2CO_3-rich solution. Sulfide oxidation at depth is possibly involved through CO_2 and H_2SO_4 production since both disseminated and massive sulfides occur in the carbonate sequence (Auler and Smart, 2003).

Stage 5: Deposition of the Silica Crust

The SiO_2-rich fluids continued to flood the MVKS during or following speleogenesis leading to the deposition of the silica crust present on the walls of the cave. Massive and fast precipitation making porous texture could be related to abrupt temperature, hydrogen potential, and oxidation/reduction potential changes caused by mixing with meteoric water from a shallower aquifer. Because calcite and dolomite on the one side, and silica on the other, have opposite solubility relationships with temperature, cooling rising waters could result both in simultaneous bedrock dissolution and silica precipitation with the SiO_2 nucleating on the dolomite. Accordingly, stages 4 and 5 do not necessarily imply a distinct temporal interval but may represent a gradually changing hydrochemical environment. Under these conditions, the influence of oxygenated meteoric groundwater could generate redox zones, in which thriving bacterial activity would favor silica precipitation (Palmer, 2007; Sauro et al., 2018). Valle (2004) has demonstrated the presence of bacterial strains in the local aquifer related to the sulfur cycle.

Stage 6: Draining of the Cave and Connection to the Surface

Eventually, the MVKS was raised from the phreatic to the vadose zone, and erosional lowering of the surface led to the interception of the cave passage, resulting in the existing entrance. This allowed for meteoric influences, causing moderate alterations of the original hypogenic features. Interactions with the atmosphere caused condensation–corrosion processes to dissolve the fabric of the dolomite, resulting in a porous layer and powdery residue that eventually detaches large pieces of silica crusts. Condensation–corrosion is more intense close to the entrance, where thermal and moisture gradients are the highest, giving rise to intense wall corrosion, silica crust detachment, and ceiling cupolas resulting from discrete airflow convections. Surface-derived clastic and organic sediments entered the cave at this stage.

A Regional Tectonic Evolution Model

We interpret our structural observations in the MVC in the frame of strike-slip tectonics acting on a system composed of a lower rigid unit, in our case the crystalline basement, overlain by a sedimentary cover made up of the Chapada Diamantina quartzite and the Salitre carbonates separated by the fine-grained sediments of the Bebedouro Fm. Based on the strike of the tilted layers and of the dominant fault zone observed in the cave, we infer an approximately north-northeast–south-southwest direction for the buried fault.

A wide range of analog models has been performed in the last decades showing the behavior of these strike-slip systems (e.g., Dooley and Schreurs, 2012). In a first stage, localized displacement in the rigid lower block is accommodated in the sedimentary cover by fractures oblique to the main fault, distributed over a wide band parallel to the fault itself. With progressing displacement, the fault migrates upward resulting in fractures aligned with the fault and localized in a narrow corridor. The overall structural evolution of the MVKS is indeed one of progressive strain localization in a transpressional setting characterized by a first stage of distributed semiductile deformation creating en echelon veins, followed by localized folding and the partly coeval development of steep barren fractures, veins, and faults (Figure 14).

Interestingly, these structural changes are associated with substantial modifications in the flow pattern and chemistry of fluids circulating in the MVKS, resulting in a complex interplay of dissolution and precipitation. Fluids documented during the distributed deformation stage (stage 1 in Table 1) were Mg rich and flowed essentially along bedding, locally facilitated by the semiductile shear zones. This suggests that fluid circulation mainly took place in the Irecê carbonate aquifer limited at the top by presently eroded impermeable strata and at the bottom by the shales and silts of the Bebedouro Fm. The activation of large, steep, mainly extensional fractures was associated with the arrival of Si-rich fluids basically flowing upward along the fractures and the steepened layers (Figure 14B). We interpret this first-order change with the upward propagation of the buried basement fault, which perched the seal formed by the Bebedouro Fm. connecting the Chapada Diamantina quartzite aquifer with the carbonates. Within this frame, aggressive SiO_2-rich fluids, possibly in combination with fluids from the limestone aquifer, caused widespread dissolution and karstification, and gradual replacement of the dolomitic walls by silica. This aggressiveness of rising fluids could be partly enhanced

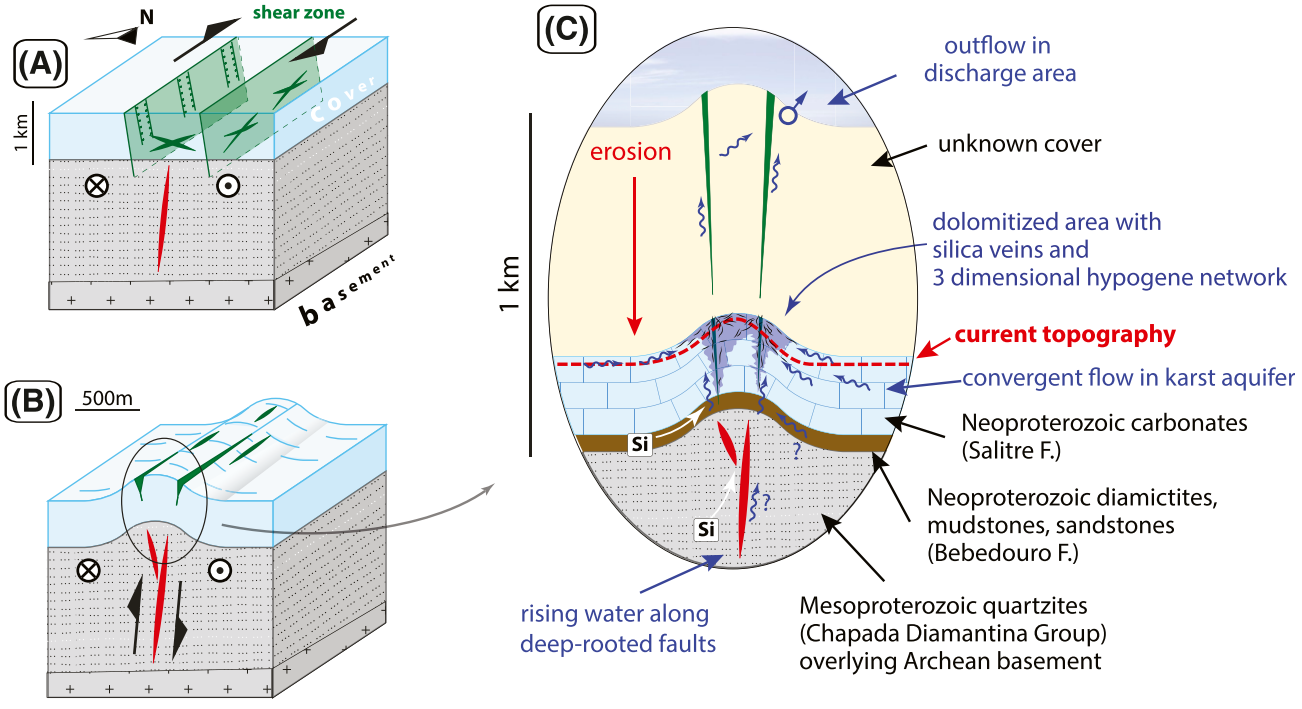

Figure 14. Evolutionary model. (A) Decimeter-scale (several inches), semiductile shear zones develop in a thrust regime distributed over a large shear zone; Mg-rich fluids flow through the entire rock mass leading to pervasive dolomitization and formation of dolomite veins. (B) Persistent strike-slip displacement along the buried fault leads to the development of a positive flower structure and associated subvertical extensional cracks, which are efficient pathways for upward fluid movement. (C) Fluids circulate along fractures and along the steepened bedding during and following steepening; eventually, recent exhumation of the cave takes place with erosion of the overlying cover. Green colors indicate the different fractures in the sedimentary cover. The buried strike-slip fault is indicated in red. F. = Formation; Si = silica.

by sulfuric acid originating from disseminated pyrite in the bedrock (Auler and Smart, 2003).

DISCUSSION

Specificity of Morro Vermelho Karst System

Hypogenic caves, which are generated by deep fluids rising along steep (strike-slip or reverse faults), have been described in other situations (Audra, 2017; Klimchouk, 2017). Such caves highlight the local development of cave porosity, focused along the guiding subvertical discontinuities where deep fluids are mixing with oxygenated shallow meteoric aquifers. The interaction between these highly aggressive fluids and the bedrock first results in focused dissolution and enlargement of cave passages (cave porosity) and second in the deposition of mineral assemblages, which can be considered as indicators of hypogene speleogenesis (generally thick drusy calcite crust, iron oxihydroxides, barite, etc.; for MVC, mainly silica). Such hypogene caves along fault zones translate in hundreds-of-meters-long vertical porosity zones, resulting in crossformational hydraulic communication between reservoirs that otherwise are isolated by aquicludes (Klimchouk, 2017). In addition, these vertical trunks focus convergent horizontal flow toward the area of ascending flow, with additional horizontal porosity growing centripetally across cave-forming zones in carbonate aquifers.

Patterns of Fluid Flow

Assessing the overall flow pattern of fluids responsible for the generation of the MVKS is key to derive models predicting the occurrence of comparable hypogenic karst systems and related mineralization in the subsurface.

Building on studies on Mississippi Valley Type deposits in the Ozark–Ouachita region of the central United States (e.g., Leach and Rowan, 1986) as well as elsewhere (Audra and Hofmann, 2004; Frazer et al., 2014; Cordeiro et al., 2018), we propose a regional evolutionary model for the MVKS that includes the interaction of processes operating at the scale of the entire Irecê Basin and that of single (strike-slip) faults.

At the basin scale, we propose that hot fluids responsible for the genesis of MVKS moved away from the São Francisco orogen during the Brasiliano orogeny (740–560 Ma) (de Brito Neves et al., 2014), driven by hydraulic head associated with recharge in the orogenic belt possibly in combination with overpressure caused by tectonic loading (e.g., Frazer et al., 2014) (Figure 15A). Flow took place from north to south along the two main aquifers of the region, namely, the Chapada Diamantina quartzite and the Salitre carbonate aquifers, separated by the aquitard of the Bebedouro Fm. This regional pattern of fluid flow is compatible with the occurrence of hypogenic karsts and of sulfate minerals (barite among others) over the entire Irecê Basin (Cazarin et al., 2019). It should be noted that the geometry of the basin at that time, prior to the Paleogene exhumation, which affected large parts of Bahia state (Japsen et al., 2012), was different from the present one and probably characterized by a significant northward dip of the Neoproterozoic layers toward the São Francisco orogen (Figure 15A). In their studies on the central United States, Leach and Rowan (1986) and Leach et al. (1991) documented fluids moving away from the orogen for hundreds of kilometers, warming up large volumes of rocks at temperatures significantly higher than those predicted by the regional gradient. Hot fluids flowing along the Salitre carbonates aquifer collected Mg on their way and were, therefore, potentially able to produce widespread dolomitization when focused along tectonized zones.

In the area of the MVKS, the general southward, aquifer-parallel flow of Mg-rich fluids interacted with a zone of coeval distributed deformation (possibly hundreds of meters wide) developing on top of a deeper, north-northeast–south-southwest–trending strike-slip fault. Widespread dolomitization took place and dolomite precipitated in the gently dipping tension gashes developed in semiductile shear zones.

With persisting displacement, the strike-slip fault, previously affecting only the crystalline basement, propagated upward intersecting the Chapada Diamantina aquifer and the Bebedouro aquitard, thereby establishing a local connection between the previously separated aquifers of the Chapada Diamantina quartzites and the Salitre carbonates and

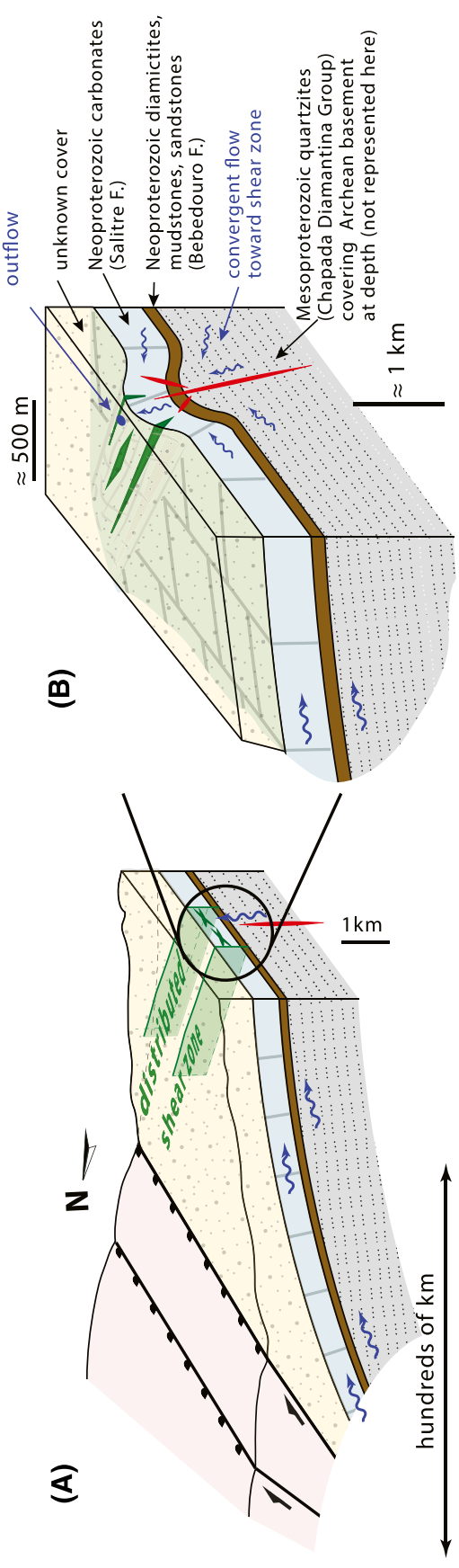

Figure 15. Regional model for the two-stage structural and flow evolutionary model of the Morro Vermelho karst system. Right: zoom to the right of the left panel showing the outflow area. The buried strike-slip fault is indicated in red; fractures in the sedimentary cover are in green. F. = Formation.

allowing for the arrival of Si-rich fluids in the MVKS. Upward flow was facilitated by the steep position of the layers tilted in association with the development of an anticline above the strike-slip fault and resulting in the precipitation of quartz in the related extensional fractures. Because fractures were steep and large, flow was very channelized, and only limited interactions and silicification took place with the country rock.

During upward flow of Si-rich fluids, speleogenesis took place, creating the MVC. Because the dissolution kinetics of calcite and dolomite have an inverse relationship to pH and temperature, and silica shows an opposite (direct) relationship, bedrock dissolution and silica precipitation are not mutually exclusive processes, although they require distinct (changing) geochemical conditions that could have happened over the long tectonic history of MVKS.

Strike-slip faults such as the one proposed here are not uncommon in the region and are older basement features that were reactivated during the Brasiliano orogeny. We propose that the location of hypogenic karst and (associated) mineralization in the Salitre Fm. of the Irecê Basin are controlled by such steep features, namely, strike-slip faults in the case of the MVKS and by reverse faults in the Toca da Boa Vista and Toca da Barriguda caves (Ennes-Silva et al., 2016; Cazarin et al., 2019) north of our study area. Structures such as strike-slip faults or steep reverse and normal faults form ideal features that can connect aquifers, promote vertical flow, and, thereby, localize karstification along structural discontinuities rather than along layering (e.g., Bradley and Leach, 2003).

Implications for Reservoir Studies

Hydrothermal dolomitization and karstification commonly associated with the deposition of exotic minerals such as barite are phenomena of primary importance in controlling the permeability of hot water and hydrocarbon reservoirs and are particularly relevant in the hydrocarbon discoveries in the subsalt of the Brazil offshore. The tectonics of these basins are obviously very different from those of the Irecê Basin, but they share the occurrence of steep strike-slip faults, which have been shown to be preferred sites of hydrothermal circulation and dolomitization not

that different from what we have observed (Davies and Smith, 2006; Feng et al., 2017).

Independently from the overall tectonic setup, the structural and related karstic events we have documented in the MVKS can be applicable to faults in deep carbonate reservoirs such as the ones imaged in the Santos Basin, offshore Brazil (Carlotto et al., 2017). Following the model generated for the MVC, strike-slip faults would be associated with an initial wholesale dolomitization followed by strain localization along steep fractures and associated intensive flow and dissolution along the fractures and the steep layers. The MVKS also shows how most of the late-stage steep fractures are (partially) open and can therefore act as major along-plane fluid pathways despite the presence of silicified veins.

CONCLUSIONS

The MVKS provides an interesting case study of speleogenesis, in which the complex interplay among tectonics, hydrochemistry, karstification and precipitation, and particularly the widespread dolomitization and (multistage?) deposition of silica resulted in a unique cave that has no parallel in the numerous caves identified so far in Brazil and beyond.

Our working hypothesis is that the MVKS started developing during the Brasiliano orogeny as a consequence of the interactions between regional fluid flow along the regional aquifers and steep strike slips propagating upward through time. Distributed deformation above a strike-slip fault and associated dolomitization are the first episodes recognized in the MVKS and occurred when fluid flow was still confined to the Salitre Fm. carbonates. The upward propagation of the strike-slip fault allowed for the upward flow of Si-rich fluids documenting the occurrence of multiple episodes of fluid upwelling, with changing chemistry and varied mineral precipitation.

The MVKS provides an instructive example of the complexities inherent to ancient deep-seated routes of dissolution and precipitation. Changes in the origin, composition, ascending path, and geochemical precipitation dynamics can lead to complex dissolution geometries and infillings that can mimic processes in carbonate oil reservoirs.

REFERENCES CITED

Audra, P., 2017, Hypogene caves in France, *in* A. B. Klimchouk, A. N. Palmer, J. de Waele, A. S. Auler, and P. Audra, eds., Hypogene karst regions and caves of the world: Berlin, Springer, p. 61–83, doi:10.1007/978-3-319-53348-3_3.

Audra, P., and B. Hofmann, 2004, Les cavités hypogènes associées aux dépôts de sulfures métalliques (MVT): Le Grotte d'Italia, v. 5, p. 35–56.

Audra, P., L. Mocochain, J.-Y. Bigot, and J.-C. Nobecourt, 2009, Morphological indicators of speleogenesis: Hypogenic speleogens, *in* A. B. Klimchouk and D. C. Ford, eds., Hypogenic speleogenesis and karst hydrogeology of artesian basins: Simferopol, Ukraine, Ukrainian Institute of Speleology and Karstology, p. 13–17.

Audra, P., and A. N. Palmer, 2015, Research frontiers in speleogenesis. Dominant processes, hydrogeologic conditions and resulting cave pattern: Acta Carsologica, v. 44, no. 3, p. 315–348, doi:10.3986/ac.v44i3.1960.

Auler, A. S., and P. L. Smart, 2003, The influence of bedrock-derived acidity in the development of surface and underground karst: Evidence from the Precambrian carbonates of semi-arid northeastern Brazil: Earth Surface Processes and Landforms, v. 28, no. 2, p. 157–168, doi:10.1002/esp.443.

Basso, M., M. C. Kuroda, L. C. S. Afonso, and A. C. Vidal, 2018, Three-dimensional seismic geomorphology of paleo-karts in the Cretaceous Macaé Group carbonates, Campos Basin, Brazil: Journal of Petroleum Geology, v. 41, no. 4, p. 513–526, doi:10.1111/jpg.12719.

Bertotti, G., S. de Graaf, K. Bisdom, B. Oskam, H. B. Vonhof, F. H. R. Bezerra, J. J. G. Reijmer, and C. L. Cazarin, 2017, Fracturing and fluid-flow during post-rift subsidence in carbonates of the Jandaíra Formation, Potiguar Basin, NE Brazil: Basin Research, v. 29, p. 836–853, doi:10.1111/bre.12246.

Besl, P. J., and N. D. McKay, 1992, Method for registration of 3-D shapes, *in* P. S. Schenker, ed., Sensor fusion IV: Control paradigms and data structures: 12-15 November 1991 Boston, Massachusetts (Proceedings of SPIE): Bellingham, Washington, International Society for Optics and Photonics, v. 1611, p. 586–607.

Bosse, M., R. Zlot, and P. Flick, 2012, Zebedee: Design of a springmounted 3D range sensor with application to mobile mapping: IEEE Transactions on Robotics, v. 28, no. 5, p. 1104–1119, doi:10.1109/TRO.2012.2200990.

Bradley, D. C., and D. L. Leach, 2003, Tectonic controls of Mississippi Valley-type lead-zinc mineralization in orogenic forelands: Mineralium Deposita, v. 38, no. 6, p. 652–667, doi:10.1007/s00126-003-0355-2.

Burchette, T. P., 2012, Carbonate rocks and petroleum reservoirs: A geological perspective from the industry: Geological Society, London, Special Publications 2012, v. 370, p. 17–37, doi:10.1144/SP370.14.

Carlotto, M. A., R. C. B. da Silva, A. A. Yamato, W. L. Trindade, J. L. P. Moreira, R. A. R. Fernandes, O. J. S. Ribeiro et al., 2017, Libra: A newborn giant in the Brazilian presalt province, *in* R. K. Merrill and C. A. Sternbach, eds.,

Giant fields of the decade 200–2010: AAPG Memoir 113, p. 165–176, doi:10.1306/13572006M1133685.
Cazarin, C. L., F. H. Bezerra, L. Borghi, R. V. Santos, J. Favoreto, J. A. Brod, A. S. Auler, and N. K. Srivastava, 2019, The conduit-seal system of hypogene karst in Neoproterozoic carbonates in northeastern Brazil: Marine and Petroleum Geology, v. 101, p. 90–107, doi:10.1016/j.marpetgeo.2018.11.046.
CloudCompare, 2019, CloudCompare (version 2.9), accessed August 24, 2020, http://www.danielgm.net/cc/release/.
Cordeiro, P. F. O., C. G. Oliveira, L. N. Paniago, G. Romagna, and R. V. Santos, 2018, The carbonate-hosted MVT Morro Agudo Zn-Pb deposit, central Brazil: Ore Geology Reviews, v. 101, p. 437–452, doi:10.1016/j.oregeorev.2018.08.002.
Davies, G. R., and L. B. Smith Jr., 2006, Structurally controlled hydrothermal dolomite reservoir facies: An overview: AAPG Bulletin, v. 90, no. 11, p. 1641–1690.
de Almeida, F. F. M., B. B. de Brito Neves, and C. Dal Ré Carneiro, 2000, The origin and evolution of the South American Platform: Earth-Science Reviews, v. 50, no. 1–2, p. 77–111, doi:10.1016/S0012-8252(99)00072-0.
de Brito Neves, B. B., R. A. Fuck, and M. M. Pimentel, 2014, The Brasiliano collage in South America: A review: Brazilian Journal of Geology, v. 44, no. 3, p. 493–518, doi:10.5327/Z2317-4889201400030010.
Delvaux, D., and B. Sperner, 2003, New aspects of tectonic stress inversion with reference to the TENSOR program: Geological Society, London, Special Publications 2003, v. 212, p. 75–100, doi:10.1144/GSL.SP.2003.212.01.06.
De Waele, J., S. Fabbri, T. Santagata, V. Chiarini, A. Columbu, and L. Pisani, 2018, Geomorphological and speleogenetical observations using terrestrial laser scanning and 3D photogrammetry in a gypsum cave (Emilia Romagna, N. Italy): Geomorphology, v. 319, p. 47–61, doi:10.1016/j.geomorph.2018.07.012.
Dooley, T. P., and G. Schreurs, 2012, Analogue modelling of intraplate strike-slip tectonics: A review and new experimental results: Tectonophysics, v. 574–575, p. 1–71, doi:10.1016/j.tecto.2012.05.030.
Ennes-Silva, R. A., F. H. R. Bezerra, F. C. C. Nogueira, F. Balsamo, A. Klimchouk, C. L. Cazarin, and A. S. Auler, 2016, Superposed folding and associated fracturing influence hypogene karst development in Neoproterozoic carbonates, São Francisco Craton, Brazil: Tectonophysics, v. 666, p. 244–259, doi:10.1016/j.tecto.2015.11.006.
Feng, M., P. Wu, Z. Qiang, X. Liu, Y. Duan, and M. Xia, 2017, Hydrothermal dolomite reservoir in the Precambrian Dengying Formation of central Sichuan Basin, Southwestern China: Marine and Petroleum Geology, v. 82, p. 206–219, doi:10.1016/j.marpetgeo.2017.02.008.
Frazer, M., F. Whitaker, and C. Hollis, 2014, Fluid expulsion from overpressured basins: Implications for Pb–Zn mineralisation and dolomitisation of the East Midlands platform, northern England: Marine and Petroleum Geology, v. 55, p. 68–86, doi:10.1016/j.marpetgeo.2014.01.004.
Goldscheider, N., J. Mádl-Szönyi, A. Eröss, and E. Schill, 2010, Thermal water resources in carbonate rock aquifers [in French]: Hydrogeology Journal, v. 18, no. 6, p. 1303–1318, doi:10.1007/s10040-010-0611-3.
Hollis, C., E. Bastesen, A. Boyce, H. Corlett, R. Gawthorpe, J. Hirani, A. Rotevatn, and F. Whitaker, 2017, Fault-controlled dolomitization in a rift basin: Geology, v. 45, no. 3, p. 219–222, doi:10.1130/G38s394.1.
Japsen, P., J. M. Bonow, P. F. Green, P. R. Cobbold, D. Chiossi, R. Lilletveit, L. P. Magnavita, and A. Pedreira, 2012, Episodic burial and exhumation in NE Brazil after opening of the South Atlantic: GSA Bulletin, v. 124, no. 5–6, p. 800–816, doi:10.1130/B30515.1.
Japsen, P., P. F. Green, J. M. Bonow, E. S. Rasmussen, J. A. Chalmers, and T. Kjennerud, 2010, Episodic uplift and exhumation along North Atlantic passive margins: Implications for hydrocarbon prospectivity, *in* B. A. Vining and S. C. Pickering, eds., Petroleum geology: From mature basins to new frontiers—Proceedings of the 7th Petroleum Geology Conference: Geological Society, London, Petroleum Geology Conference Series 2010, v. 7, p. 979–1004, doi:10.1144/0070979.
Klimchouk, A. B., 2007, Hypogene speleogenesis: Hydrogeological and morphogenetic perspective: Carlsbad, New Mexico, National Cave and Karst Research Institute, 118 p.
Klimchouk, A. B., 2009, Morphogenesis of hypogenic caves: Geomorphology, v. 106, no. 1–2, p. 100–117, doi:10.1016/j.geomorph.2008.09.013.
Klimchouk, A. B., 2012, Speleogenesis, hypogenic, *in* W. B. White and D. C. Culver eds., Encyclopedia of caves, 2nd ed.: Cambridge, Massachusetts, Academic Press, p. 748–765, doi:10.1016/B978-0-12-383832-2.00110-9.
Klimchouk, A. B., 2017, Types and settings of hypogenic karst, *in* A. Klimchouk, A. N. Palmer, J. De Waele, A. S. Auler, and P. Audra eds., Hypogene karst regions and caves of the world: Berlin, Springer, p. 1–39, doi:10.1007/978-3-319-53348-3_1.
Laureano, F. V., I. Karmann, D. E. Granger, A. S. Auler, R. P. Almeida, F. W. Cruz, N. M. Strícks, and V. F. Novello, 2016, Two million years of river and cave aggradation in NE Brazil: Implications for speleogenesis and landscape evolution: Geomorphology, v. 273, p. 63–77, doi:10.1016/j.geomorph.2016.08.009.
Leach, D. L., G. S. Plumlee, A. H. Hofstra, G. P. Landis, E. L. Rowan, and J. G. Viets, 1991, Origin of late dolomite cement by CO2 saturated deep basin brines: Evidence from the Ozark region, central United States: Geology, v. 19, no. 4, p. 348–351, doi:10.1130/0091-7613(1991)019<0348:OOLDCB>2.3.CO;2.
Leach, D. L., and E. L. Rowan, 1986, Genetic link between Ouachita foldbelt tectonism and the Mississippi Valley-type lead-zinc deposits of the Ozarks: Geology, v. 14, no. 11, p. 931–935, doi:10.1130/0091-7613(1986)14<931:GLBOFT>2.0.CO;2.
Lowell, R. P., P. Van Capellen, and L. N. Germanovich, 1993, Silica precipitation in fractures and the evolution of permeability in hydrothermal upflow zones: Science, v. 260, no. 5105, p. 192–194, doi:10.1126/science.260.5105.192.
Magalhães, A. G. C., G. P. Raja Gabaglia, C. M. S. Scherer, M. B. Bállico, F. Guadagnin, E. Bento Freire, L. R. Silva

Born, and O. Catuneanu, 2016, Sequence hierarchy in a Mesoproterozoic interior sag basin: From basin fill to reservoir scale, the Tombador Formation, Chapada Diamantina Basin, Brazil: Basin Research, v. 28, no. 3, p. 393–432, doi:10.1111/bre.12117.

Martin, J. T., and R. P. Lowell, 2000, Precipitation of quartz during high-temperature, fracture-controlled hydrothermal upflow at ocean ridges: Equilibrium versus linear kinetics: Journal of Geophysical Research, v. 105, no. B1, p. 869–882, doi:10.1029/1999JB900342.

Misi, A., and J. R. Kyle, 1994, Upper Proterozoic carbonate stratigraphy, diagenesis and stromatolitic phosphorite formation, Irece Basin, Bahia, Brazil: Journal of Sedimentary Research, v. 64, no. 2a, p. 299–310.

Misi, A., and J. Veizer, 1998, Neoproterozoic carbonate sequences of the Una Group, Irecê Basin, Brazil: Chemostratigraphy, age and correlations: Precambrian Research, v. 89, no. 1–2, p. 87–100, doi:10.1016/S0301-9268(97)00073-9.

Osborne, R. A. L., 2001, Halls and narrows: Network caves in dipping limestone, examples from eastern Australia: Cave and Karst Science, v. 28, no. 1, p. 3–14.

Palmer, A. N., 2000, Hydrogeologic control of cave patterns, *in* A. B. Klimchouk, D. C. Ford, A. N. Palmer, and W. Dreybrodt, eds., Speleogenesis: Evolution of karst aquifers: Huntsville, Alabama, National Speleological Society, p. 77–90.

Palmer, A. N., 2007, Cave geology: Dayton, Ohio, Cave Books, 454 p.

Plotnick, R. E., F. Kenig, and A. Scott, 2015, Using the voids to fill the gaps: Caves, time and stratigraphy: Geological Society, London, Special Publications 2015, v. 404, p. 233–250.

Reijmer, J. J. G., J. H. ten Veen, B. Jaarsma, and R. Boots, 2018, Seismic stratigraphy of Dinantian carbonates in the southern Netherlands and northern Belgium: Netherlands Journal of Geosciences, v. 96, no. 4, p. 353–379, doi:10.1017/njg.2017.33.

Reis, H., C. Gomes, D. Fragoso, and M. Kuchenbecker, 2013, The epidermal belt of forefathers of the Irecê Basin, São Francisco Craton: Main structural elements and analogical physical modeling: USP Geology, Scientific Series, v. 13, no. 4, p. 125–139, doi:10.5327/Z1519-874X201300040007.

Rimstidt, J. D., and H. L. Barnes, 1980, The kinetics of silica-water reactions: Geochimica et Cosmochimica Acta, v. 44, no. 11, p. 1683–1699, doi:10.1016/0016-7037(80)90220-3.

Sampaio, A. R., A. J. D. Rocha, R. A. Santos, and J. T. Guimaraes, 2001, Sheet Jacobina SC.24-Y-C: Salvador, Bahia, Brasilia, Programa Levantamentos Geologicos Basicos do Brasil, Rio de Janeiro, Companhia de Pesquisa de Recursos Minerais, 1 CD-ROM, scale 1:250.000.

Sauro, F., M. Cappelletti, D. Ghezzi, A. Columbu, P.-Y. Hong, H. M. Zowawi, C. Carbone et al., 2018, Microbial diversity and biosignatures of amorphous silica deposits in orthoquartzite caves: Scientific Reports, v. 8, 17569, 14 p., doi:10.1038/s441598-018-35532-y.

Trompette, R., A. Uhlein, M. E. da Silva, and I. Karman, 1992, The Brasiliano São Francisco craton revisited (central Brazil): Journal of South American Earth Sciences, v. 6, no. 1–2, p. 49–57, doi:10.1016/0895-9811(92)90016-R.

Valle, M. A., 2004, Hidroquímica do Grupo Una (Bacias de Irecê e Salitre): Um exemplo da ação de ácido sulfúrico no sistema cárstico, Ph.D. thesis, São Paulo, Brazil, University of São Paulo, 122 p.

Zhu, H., X. Zhu, and H. Chen, 2017, Seismic characterization of hypogenic karst systems associated with deep hydrothermal fluids in the Middle-Lower Ordovician Yingshan formation of the Shunnan area, Tarim Basin, NW China: Geofluids, v. 2017, 8094125, 13 p., doi:10.1155/2017/8094125.

Zlot, R., and M. Bosse, 2014, Three-dimensional mobile mapping of caves: Journal of Caves and Karst Studies, v. 76, no. 3, p. 191–206, doi:10.4311/2012EX0287.